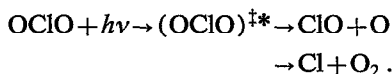


Femtosecond real-time probing of reactions. XI. The elementary OCIO fragmentation

T. Baumert,^{a)} J. L. Herek, and A. H. Zewail
Arthur Amos Noyes Laboratory of Chemical Physics,^{b)} California Institute of Technology,
Pasadena, California 91125

(Received 23 April 1993; accepted 1 June 1993)

Femtosecond reaction dynamics of OCIO in a supersonic molecular beam are reported. The system is excited to the A^2A_2 state with a femtosecond pulse, covering a range of excitation in the symmetric stretch between $v_1=17$ to $v_1=11$ (308–352 nm). A time-delayed femtosecond probe pulse ionizes the OCIO, and OCIO^+ is detected. This ion has not been observed in previous experiments because of its ultrafast fragmentation. Transients are reported for the mass of the parent OCIO as well as the mass of the ClO. Apparent biexponential decays are observed and related to the fragmentation dynamics:



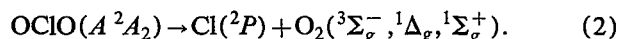
Clusters of OCIO with water $(\text{OCIO})_n(\text{H}_2\text{O})_m$ with n from 1 to 3 and m from 0 to 3 are also observed. The dynamics of the fragmentation reveal the nuclear motions and the electronic coupling between surfaces. The time scale for bond breakage is in the range of 300–500 fs, depending on v_1 ; surface crossing to form new intermediates is a pathway for the two channels of fragmentation: $\text{ClO} + \text{O}$ (primary) and $\text{Cl} + \text{O}_2$ (minor). Comparisons with results of *ab initio* calculations are made.

I. INTRODUCTION

The gas phase photodissociation mechanisms of OCIO in the near-UV region have stimulated copious experimental and theoretical studies (for recent references, see Refs. 1–13) due in part to its possible role in the depletion of ozone in the Antarctic stratosphere.¹⁴ The absorption spectrum of OCIO ($A^2A_2 \leftarrow X^2B_1$) spans from 475 to 273 nm (Refs. 15 and 16) (Fig. 1). At all absorption wavelengths, the major dissociation channel is found to be



whereas a minor channel is



Since the O atom formed in reaction (1) could react with O_2 molecules in the atmosphere to produce O_3 , this dissociation pathway would lead to a null cycle in stratospheric ozone depletion. Reaction (2), however, represents a mechanism for halogen-catalyzed conversion of O_3 to O_2 . To understand the photodissociation mechanism of OCIO, different experimental techniques have been applied.

In describing the elementary nuclear motions of OCIO fragmentation, three coordinates must be considered—the symmetric stretch v_1 , the bend v_2 , and the asymmetric stretch v_3 (see Table I). Generally, for a given bend configuration, a wave packet on a single potential energy surface (PES) will evolve along the reaction coordinate from the bound symmetric stretch region of the PES (Fig. 2). Since the pump is not energetically broad enough to span levels of v_1 , a localized wave packet is not created along the

symmetric stretch coordinate. If a wave packet could be generated, the problem becomes analogous to the case of HgI_2 , where coherent nuclear motion (Fig. 3) to yield $\text{HgI} + \text{I}$ was observed and studied.^{17–19} For OCIO, the problem is more complicated, however, due to the fact that several nearby potentials may be involved.

In this paper, in the series, we report studies of the ultrafast dynamics of OCIO elementary fragmentation using the techniques of femtosecond transition-state spectroscopy (for reviews, see Refs. 20 and 21). Of particular relevance here is the use of multiphoton ionization and mass spectrometry,^{22–26} which makes it possible to observe the parent ion of OCIO (i.e., OCIO^+) hitherto undetected by previous nanosecond experiments. We follow the initial nuclear motion and measure the real-time dissociation to different fragments. In the range of $v_1=11$ –17, bond breakage times are typically 300–500 fs, while the initial decay ranges from 30 to 120 fs. We relate these observations to the nature of the dynamics and to recent *ab initio* calculations of the PESs. We also report results on the detection of one of the fragments (ClO) and preliminary studies of OCIO when selectively solvated with water.

The outline of the paper is as follows: In Sec. II, a brief description of the experiment is provided, followed by results and data analysis in Sec. III. The discussion presented in Sec. IV includes previous spectroscopic and beam work on OCIO as well as our contribution relating the femtosecond dynamics and mechanism of dissociation. Concluding remarks are given in Sec. V.

II. EXPERIMENT

The femtosecond laser apparatus has been described in detail previously²⁷ and is discussed only briefly here. Fem-

^{a)}Deutsche Forschungsgemeinschaft (DFG) postdoctoral fellow.

^{b)}Contribution no. 8774.

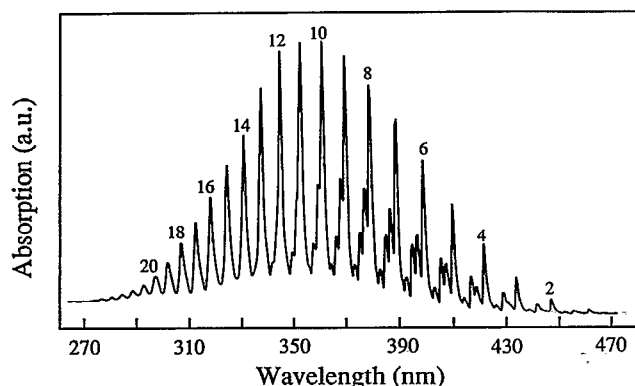


FIG. 1. The medium-resolution absorption spectrum of OCIO from Ref. 16. Assignments are taken from Ref. 15.

tosecond pulses were generated from a colliding pulse mode-locked (CPM) ring dye laser and amplified by a Nd:YAG-pumped pulsed dye amplifier (PDA). The recompressed output pulses had an (unattenuated) energy of 0.2–0.3 mJ at a repetition rate of 20 Hz. The pump wavelengths in the range from 308 to 312 nm were generated by frequency doubling a part of the PDA output in a 0.2 mm thick KDP crystal; for these wavelengths, the CPM was tuned by proper adjustment of the saturable absorber concentration. In order to obtain the wavelength range from

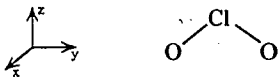
312 to 352 nm, we focused part of the PDA output on a D₂O cell to produce a white light continuum. With 10 nm bandwidth interference filters, we selected the desired wavelengths from 624 to 704 nm; this light was further amplified in a longitudinally pumped dye cell before being doubled in a KDP crystal. For the multiphoton ionization (MPI) probe, we used the remaining output of the PDA at 620 nm.

The pump and probe beams, with proper attenuation and parallel or perpendicular polarization, were delayed in time relative to one another in a Michelson interferometer and were then recombined collinearly and focused onto the OCIO molecular beam. Before entering the molecular beam, we routinely recorded autocorrelations of the probe (~ 80 fs sech²) and cross correlations between pump and probe (~ 190 fs).

The supersonic molecular beam consisted of a pulsed nozzle with an orifice diameter of 0.3 mm. MPI experiments on the skimmed molecular beam were carried out in a differentially pumped ionization chamber about 12 cm downstream from the nozzle. The time-of-flight (TOF) detector had a field-free drift tube with a mass resolution of $\sim 1:150$. The molecular beam, the lasers, and the TOF detection axes were mutually perpendicular. A sketch of the experimental arrangement is shown in Fig. 4.

OCIO was produced *in situ* by flowing a 3.5% Cl₂/He mixture through a U tube packed with glass beads and

TABLE I. OCIO in C_{2v} geometry.

					
Frequency $\bar{\nu}$ (cm ⁻¹) [Period (fs)]	ν_1	ν_2	ν_3	T_e (eV)	Reference
X^2B_1	963.5 (35)	451.7 (74)	1123.0 (29)		a
2B_2	815.0 (41)	319.5 (104)	520 (64)	1.98	b
2A_1	696.5 (48)	311.3 (107)	1474 (23)	2.60	b
A^2A_2	713.2 (47)	287.1 (116)	401.5 (83)	2.68	c
Symmetry of normal vibrations					
Symmetric stretch (ν_1)	a_1				
Bend (ν_2)	a_1				
Asymmetric stretch (ν_3)	b_2				
Electric dipole selection rules					
$A^2A_2 \leftarrow X^2B_1$	Parallel polarized				
$^2A_1 \leftarrow X^2B_1$	Perpendicular polarized				
$^2B_2 \leftarrow X^2B_1$	Forbidden				
Allowed pairs of electronic states for vibronic coupling					
A_2-B_1					
A_1-B_2					

^aTaken from Ref. 60.

^bTaken from Ref. 12.

^cVibrational constants were derived from Ref. 9. T_e was derived from Refs. 12 and 60.

^dFor rotations, see Ref. 62.

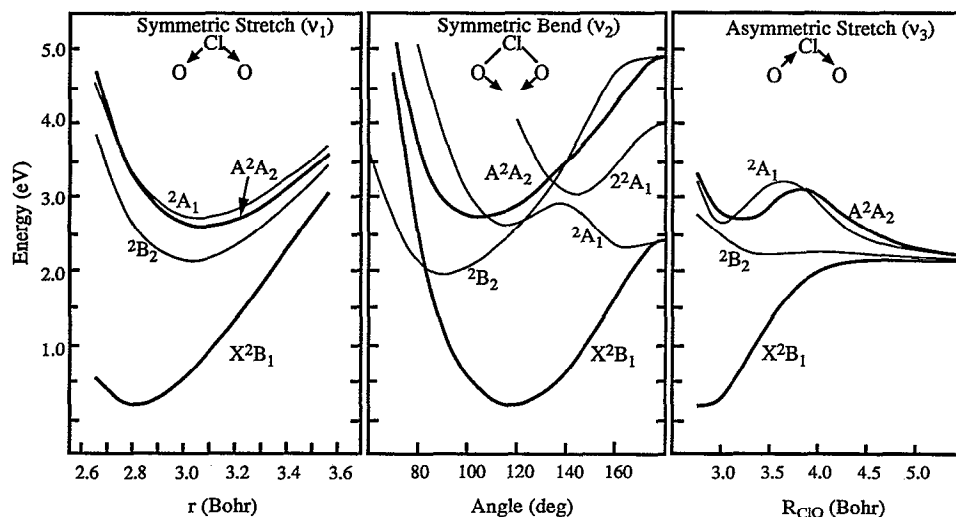


FIG. 2. Cuts through “*ab initio*” potential energy surfaces from Ref. 12. All symmetry notations are for C_{2v} geometry. The symmetric stretch potential is shown for a fixed valence angle of 106.4° (calculated A^2A_2 equilibrium angle; experimental value 106.2°) (1 bohr = 0.529 \AA).

NaClO_2 , following the procedure of Derby and Hutchinson.²⁸ In order to be below the detonation limit of OCIO, a constant total backing pressure of 1.5 atm was maintained for the expansion of OCIO. In concentrations in excess of 10% of atmospheric pressure, OCIO is easily detonated by sources of initiation such as sunlight, heat, or electric discharge.²⁸

III. RESULTS AND ANALYSIS

In Fig. 5, a TOF spectrum is shown for an excitation wavelength centered at 329 nm. This corresponds to the absorption peak 14 in Fig. 1, which is labeled spectroscopically as the (14 0 0) band. The probe laser (620 nm) was set at a time delay of 170 fs. A prominent feature in this resonance-enhanced multiphoton ionization (REMPI) TOF spectrum is the two OCIO isotopes. As mentioned above, OCIO^+ ions have not been observed previously in nanosecond-laser REMPI experiments.¹³ The products in this spectrum are the two ClO isotopes. Sufficient cooling

of our sample is obtained, as evident by the onset of the cluster formation. We also observe $(\text{OCIO})_n$ clusters with $n = 1-3$ and $(\text{OCIO})_n (\text{H}_2\text{O})_m$ clusters with $n, m = 1-3$. No additional water was used in the heterogeneous OCIO-water cluster formation; the inherent moisture of the NaClO_2 provided enough water vapor pressure for clustering. All cluster mass channels are split due to the two Cl isotopes. The $(\text{H}_2\text{O})_5$ cluster, prominent in the electron impact mass spectrum of Vaida *et al.*,¹³ is not seen in this femtosecond pump-probe REMPI spectrum under the above conditions.

The femtosecond experiments on the mass-selected parent OCIO or fragments involve the following scheme of energy and mode excitations (Fig. 6): The initial excitation is from the (0 0 0) state (with relatively low hot-band excitation) of the X^2B_1 ground state of OCIO to the A^2A_2 state (the region between 3.5–4 eV). In the absorption spectra of Fig. 1, this excitation corresponds to bands 11 (351.3 nm) to 17 (311.5 nm). This transition is parallel

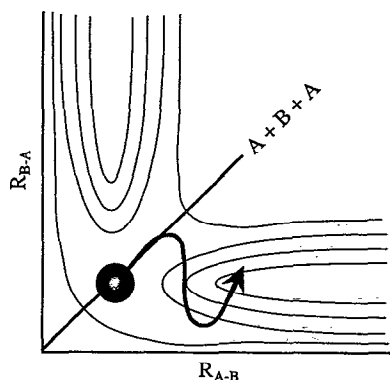


FIG. 3. A schematic of an ABA potential energy surface. The filled circle represents the localized wave packet that moves with a wide oscillatory motion into the asymmetric stretch dissociation channel to form $AB + A$ (OCIO vs IHgI case discussed in the text).

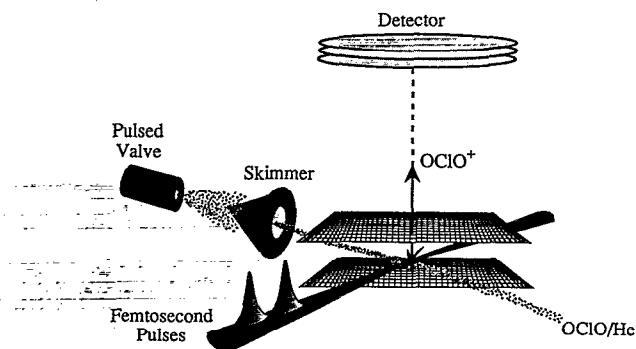


FIG. 4. A schematic of our experimental setup. The collinear femtosecond lasers, the molecular beam, and the TOF axes are all mutually perpendicular.

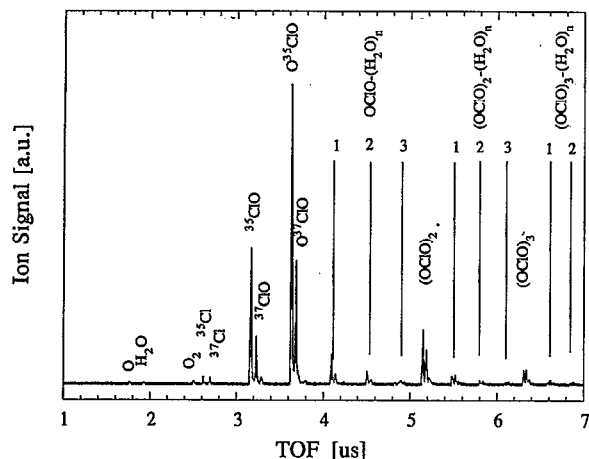


FIG. 5. The TOF spectrum taken in a femtosecond pump-probe arrangement. Note that the prominent masses are the OCIO parent and the ClO product.

polarized; the perpendicular polarized transition into the 2A_1 state, in principle allowed, has not been observed experimentally.¹³ The transition to the 2B_2 state is dipole forbidden. In the energy range 7–8 eV (two pump photon excitation), only one-photon absorption spectra are reported,^{29,30} with very short progressions.³⁰ As discussed below, two-photon excitations are minimized.

It takes four probe photons at 620 nm to ionize the system. A continuous increase of the one-photon absorption cross-section from 6 up to 25 eV was measured by Flesch *et al.*,²⁹ indicating that the probe laser ionization involves a REMPI process (*vide infra*). The ionization potential of OCIO is 10.33 ± 0.02 eV.²⁹ As shown in Fig 6, at least one additional probe photon (making a total of at least five probe photons) is required to reach the ionic fragmentation channel. The threshold for $\text{ClO}^+ (^3\Sigma^-) + \text{O} (^3P)$ is measured to be 13.45 ± 0.04 eV.²⁹ The D_0 value

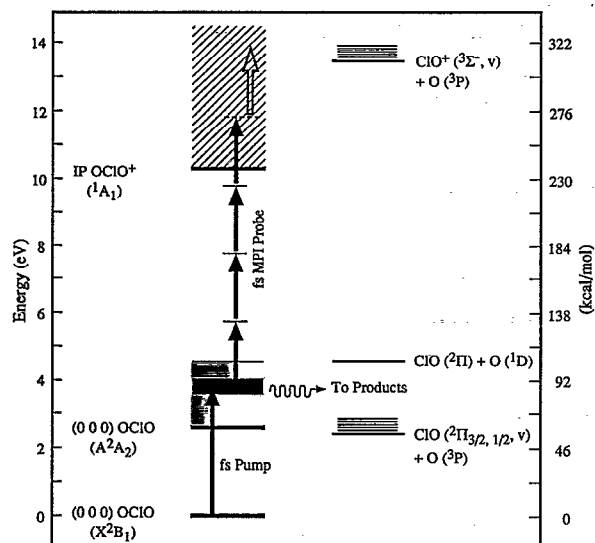


FIG. 6. A pump-probe excitation scheme for studying OCIO fragmentation dynamics.

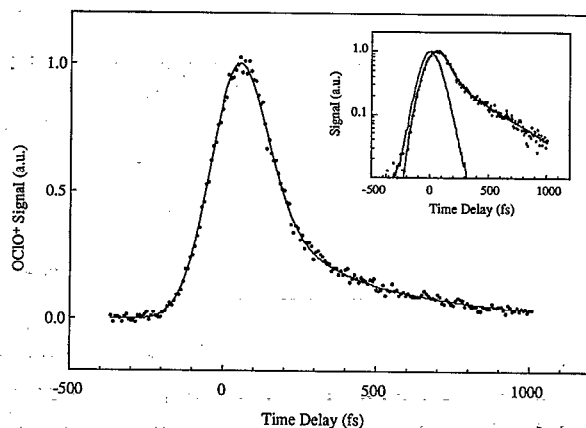


FIG. 7. A typical femtosecond transient taken on the O^{35}ClO parent mass. The solid line is a double exponential fit to the data including convolution with the cross correlation. The insert shows the decay on a logarithmic signal axis, in which the biexponential character is evident. For comparison, the symmetric cross correlation is also shown in the insert.

for the neutral $\text{ClO} (^2\Pi) + \text{O} (^3P)$ asymptote is given to be 55.2 ± 2 kcal/mol,³¹ corresponding to ~ 2.4 eV. Taking into account the fact that the ClO fragments are vibrationally excited to the $v''=3-6$ range⁷ and knowing the vibrational frequency of ClO in its ground state (~ 0.1 eV),³² our total available energy with respect to ground state fragmentation is ~ 1 eV. Energetically, the next higher fragmentation channel leading to $\text{ClO} (^2\Pi) + \text{O} (^1D)$ would require a threshold energy of ~ 4.5 eV. Hence, the fragmentation channels leading to electronically excited ClO or excited O may be excluded from further consideration.

Typical femtosecond transients taken on O^{35}ClO and ^{35}ClO are shown in Figs. 7 and 8. The transients were taken at a pump wavelength of 329 nm at band 14 in Fig. 1. First we consider the O^{35}ClO transient in Fig. 7. From

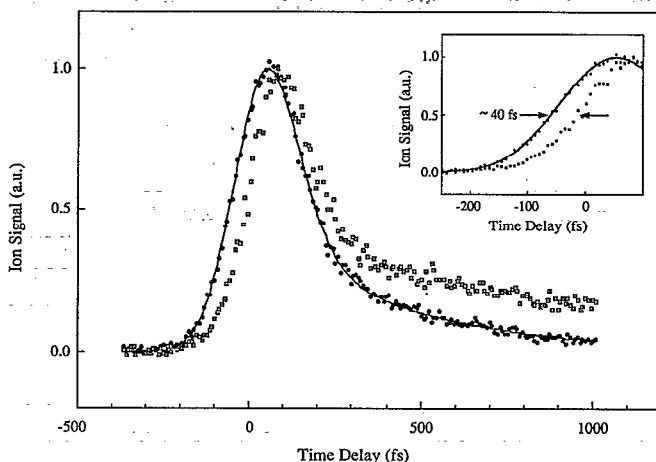


FIG. 8. The OCIO^+ transient (dots) and ClO^+ transient (squares) taken under the same experimental conditions. Note the similar shape of the transient, but the time shift in the rise and the final value at longer pump-probe delay times in the ClO^+ transient (see the text).

the insert, plotted on a logarithmic scale, it is evident that the transient shows a biexponential decay. The cross correlation, also shown in the insert, is symmetric and different from the initial decay. The time constants, derived from a molecular response function of the type

$$M(t) = Ae^{-t/\tau_1} + Be^{-t/\tau_2} \quad (A + B = 1), \quad (3)$$

are $\tau_1 \sim 50$ fs, $\tau_2 \sim 400$ fs, and $A \sim 0.89$ for this transient. These results depend on the initial excitation energy and are not consistent with a simple sum of a decay and an off-resonance ionization signal (*vide infra*). The values for τ_2 are much larger than our response function; in order to obtain accurate values of τ_1 , we convoluted the transient form of Eq. (3) with the measured cross correlation taken carefully before and after the experiments (Fig. 7).

Care was taken in considering several control experiments. First, according to the energetics of this system (Fig. 6), the process requires one pump photon and four probe photons. The laser intensities were therefore adjusted such that the pump laser alone did not produce an appreciable MPI signal. Typical values were a maximum of 10% MPI signal from the pump laser alone relative to the MPI level of the stronger probe laser. The maximum signal enhancement was then typically two to three times greater than the time-independent background consisting of the sum of pump and probe MPI levels.

Second, while the pump (alone without the probe) MPI background signal vs intensity showed an approximate quadratic power dependence, the total signal due to pump plus probe vs pump laser intensity showed an approximate linear power dependence. Probe laser intensity studies showed a similar behavior.

Third, the ratio A/B of the amplitudes of the two time constants [Eq. (3)] did not change by attenuating the pump laser, as would be expected if one of the time constants were due to a two-photon or off-resonance excitation. It is known from similar work that the pump laser intensity does not affect the time constants in a femtosecond MPI process (where one-photon excitation dynamics and two-photon excitation dynamics contribute to the observed transient ionization signal), yet the *ratio* of these contributions is very sensitive to intensity.³³ A further indication of the approximate linearity of the total signal in these experiments is that the rise of the transients could be fitted nicely to the cross correlation (measured in front of the molecular beam apparatus).

Fourth, parallel or perpendicular polarization of our lasers had no significant influence on our transients, neither on the observed time constants nor on the A/B ratio. Most of the experiments were performed with perpendicular polarization.

Tuning the laser from ν_1 band 17 to band 11 resulted in an increase of τ_1 from about 30 to about 120 fs. The second time component also increased from about 300 to ~ 500 fs. This increase in the time constants with respect to lower excitation energies is accompanied by a decrease of the A/B ratio of the two time components; the fast component was always found to be the dominant contribution. These trends are summarized in Fig. 9.

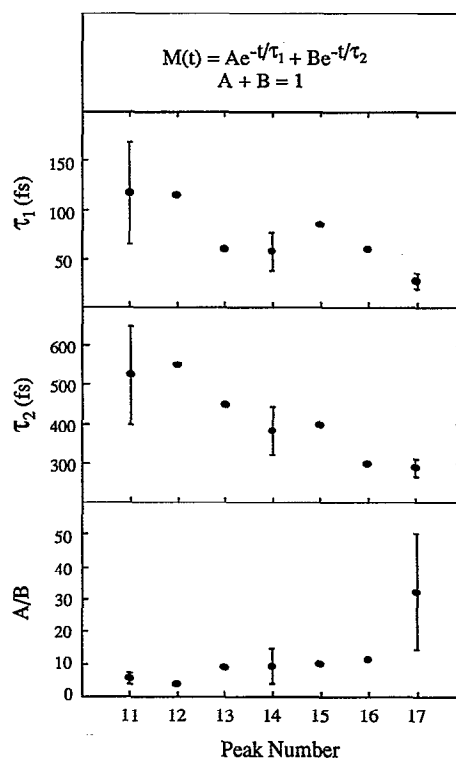


FIG. 9. Pump wavelength dependence of the two time constants and the A/B ratio. The peak numbers correspond to the numbers given in Fig. 1 for the vibrational stretch quantum number. The points with error bars represent data sets that include enough measurements to give a meaningful standard deviation.

From the high-resolution work of Vaida *et al.*,⁹ it is known, at least for the low excitation regime, that to the blue side of every pure symmetric stretch excitation, a $(\nu_1 0 2)$ band is observed (in addition to other combination bands). The rotational line broadening analysis suggests significant broadening of the $(\nu_1 0 2)$ band compared to the symmetric stretch alone $(\nu_1 0 0)$.¹⁰ Tuning the central wavelength of our femtosecond-pump laser up to 4 nm to the blue side of the $(14 0 0)$ band did not yield significant changes in the two time constants. Thus, the “mode selectivity” seen in the low-excitation regime seems to be blurred in the high-excitation region of the spectrum, where mode-specific structure also appears to “wash out” in the low-resolution spectrum (Fig. 1). Note that this small tuning is comparable to the full width at half-maximum (FWHM) (~ 3.5 – 4 nm) of the pulse. If the transient were composed of a superposition of two components (decay and off-resonant ionization), we would have expected changes in the A/B ratio of the fast and slow components associated with tuning the central wavelength of the pump from a maximum in the low-resolution spectrum to as much as 4 nm away.

In addition to the above results on the parent molecule, we also studied the transients of the observed mass fragments. The ClO transient in Fig. 8 resembles the OCIO transient, also shown in this figure, but there are two differences. First, the rise of the ClO transient is shifted with

respect to the rise of the OCIO transient by 20–40 fs. This shift is real, as the ClO transients were recorded with the same experimental conditions as the OCIO transients, by only changing the detection electronics (gate of a boxcar) from the mass of the OCIO to the mass of the ClO. The shift is displayed in the inset of Fig. 8. Second, the final value of ClO^+ reaches an asymptote of 15% to 25% of the total signal, as seen in Fig. 8. On a time scale of up to 15 ps (the maximum pump–probe delay in these experiments), this final value remained constant.

Power dependence studies also showed an approximate linear dependence of the total signal with respect to pump and probe laser intensities. The fact that the ClO signal reaches a final value is consistent with the expectation that the neutral fragmentation of OCIO leads to $\text{ClO} + \text{O}$ after the pump–pulse excitation. As the I.P. of ClO is 11.01 ± 0.01 eV,³⁴ it takes six photons of our probe laser to ionize this species. This nonzero ClO signal at all excitation wavelengths (including 308 nm, where previous femtosecond experiments were performed) is formed on the femtosecond time scale and remains for long times.

For the short-time behavior, the OCIO and ClO transients match in shape, but, of course, with the time shift. This suggests that they have the same origin; they are directly related to the fragmentation dynamics of the OCIO. Note that only one additional probe photon is needed to reach the ionic fragmentation channel from the ionic OCIO ground state (Fig. 6). Typical time scales in the ionic ground state are ~ 35 fs for the symmetric stretch and ~ 70 fs for the bending motion.²⁹ These times correspond to the observed shift of about 20–40 fs of the ClO^+ transient with respect to the OCIO^+ transient. We therefore suggest that the time shift is due to the propagation of a wave packet in the OCIO^+ ground state from the region initially excited by four probe photons into a region where the Franck–Condon (FC) factors are more favorable for the $\text{ClO}^+ + \text{O}$ fragmentation. Absorption of a fifth probe photon would then lead to such fragmentation. The transient of the ClO^+ thus reflects both the neutral product formation and then ionization (long-time constant level) and the parent OCIO ionization and subsequent ion fragmentation with decay (short time behavior).

IV. DISCUSSION

A. Spectroscopic and beam studies

In the high resolution absorption spectra of OCIO by McDonald and Innes³ and Michielsen *et al.*,² the rotational structure of the symmetric-stretch progression was investigated for $v_1 = 1$ –5. It was found that the rate of “predissociation” (*vide infra*) depends on the spin state prepared. The rate is greater for the F_1 ($J = N + 1/2$) state than for the F_2 ($J = N - 1/2$) state and is independent of the rotational state of the initially excited molecule. In addition, it was found that for $v_1 < 3$, the rate of predissociation from the states ($v_1 0 0$) is independent of v_1 , but for $v_1 > 3$, the rate increases with v_1 . For example, the lifetime of the F_1 component in the (0 0 0) state is given to be 67 ± 14 ps, while for the (5 0 0) band, 28 ± 1 ps is re-

ported.² It is further noted that the bending mode shows faster predissociation rates at comparable energies. According to the two-dimensional cuts through the “*ab initio*” PESs along the symmetric stretch, bend, and asymmetric stretch coordinates calculated by Peterson and Werner¹² (Fig. 2), the system is bound along the first two and unbound along the asymmetric stretch.

Direct vibronic coupling of the 2A_2 state to the close lying 2B_2 and 2A_1 states is forbidden for this triatomic in C_{2v} symmetry, while allowed to the 2B_1 ground state.³⁵ McDonald and Innes³ have argued that it is unlikely that the 2B_1 ground state couples with the prepared A^2A_2 state, as the observed vibrational and spin dependencies of the rotational linewidths could not be reasonably explained by such coupling of the excited manifold. As the bending mode is promoting the predissociation and the 2B_2 state is strongly bent (Fig. 2), Michielsen *et al.*² and McDonald and Innes³ concluded that the A^2A_2 state mixes with the 2B_2 state by spin–orbit coupling before proceeding to dissociation. Recent calculations by Peterson and Werner¹² of the PES and a closer analysis of the possible excited-state interactions with respect to symmetric stretch, bend, and asymmetric stretch coordinates prefer the 2A_1 state as the state from which the predissociation proceeds.

Vaida and co-workers¹⁰ provided the analysis of rotational line broadening involving ($v_1 0 0$), ($v_1 1 0$), and ($v_1 0 2$) bands of OCIO, extending the range from $v_1 = 4$ –10. The absorption spectrum was measured directly using jet-cooled Fourier transform ultraviolet spectroscopy.^{4,9} They observed an increase in (fitted) rotational linewidths, and thus a decrease in the corresponding lifetimes from about 20 ps at (5 0 0) to about 4 ps at (10 0 0) (see Fig. 3 in Ref. 10). In studying modes involving bending excitation, linewidths were found to be four to five times broader than for the symmetric stretch alone at the same energy. It was also found that combinations involving v_1 with $2v_3$ broaden more rapidly than combinations of v_1 with v_2 . The experimental observations were explained via interactions of the A^2A_2 state with both the 2A_1 and 2B_2 states, analogous to the earlier work of McDonald and Innes³ and Michielsen *et al.*² In the excitation region higher than $v_1 = 10$, it is reported that the linewidths appear to reach a limit and become fairly constant with lifetimes. A more detailed analysis of rotational linewidth broadening is not given in this energy region, as the individual rotational linewidths become too broad and thus only the rotational envelopes are discernible (Fig. 10). Estimates of the lifetimes, however, are given at 303 nm (v_1 between 18 and 19) to be ~ 1 ps, and for the $v_3 = 4$ level at 333 nm, linewidths of ~ 100 cm^{-1} (~ 50 fs) were reported with the note that these bands are disappearing into noise.¹⁴

Experiments involving nanosecond-laser REMPI techniques have also been reported: Vaida’s group recorded spectra in the range from 335 to 370 nm which focused on the ClO^+ and Cl^+ channel,⁷ however, the parent OCIO^+ was not seen.¹³ Ionization and fragmentation are two competing channels, and with nanosecond pulses, “channel switching,” discussed by Schlag and Neusser³⁶ and Taylor and Johnson,³⁷ can lead to ionization of fragments and not

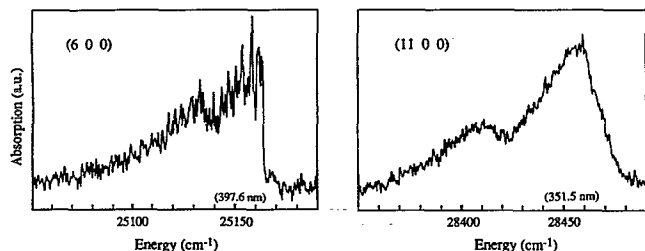


FIG. 10. High-resolution spectra of the (6 0 0) and (11 0 0) bands from Ref. 4. At the (6 0 0) band, there are resolved rotational structures. For these bands, contours were fitted to give estimates of the lifetimes. The two peaks in the (11 0 0) band, and also the (6 0 0) band, are due to the two Cl isotopes.

of the parent neutral. Such behavior has previously been demonstrated in methyl iodide,^{23,26} where the CH_3I^+ and fragment I^+ were observed to vary in intensity depending on the delay time between the pump and MPI pulses. Another example comes from the work of Gerber's group³⁸ on Na_n cluster resonances. When, e.g., $n > 4$, the absorption spectra of the Na_n clusters could not be measured directly by nanosecond-laser REMPI techniques due to the fast fragmentation processes of the excited intermediate states. However, femtosecond-laser REMPI techniques were successful in observing these resonances as well as determining the lifetimes of the intermediate states directly in the time domain via pump-probe experiments. The product analysis in Vaida's group's work⁷ indicated that for the $\text{O}(^3P) + \text{ClO}(X^2\Pi)$ fragmentation, the ClO molecules were released vibrationally excited ($v'' = 3-6$).

They also observed Cl^+ REMPI action spectra in the region 360–363 nm and attributed this observation to an isomerization of OCIO to ClOO, which subsequently dissociates to $\text{Cl} + \text{O}_2$. The quantum yield for Cl formation was reported by Lawrence *et al.*⁶ to be less than 5×10^{-4} between 359 and 368 nm, an upper limit as they did not actually observe $\text{Cl} + \text{O}_2$. A further REMPI experiment was reported by Bishenden *et al.*⁸ who used a tunable dye laser to excite OCIO in the wavelength range 355–370 nm and probed Cl via a (2+1) REMPI process near 235 nm. In contrast to the work of Lawrence *et al.*, the quantum yield near 362 nm for the formation of Cl was given to be 0.15 ± 0.10 . The REMPI spectrum of Bishenden *et al.* reproduces the OCIO absorption spectrum, suggesting that the Cl^+ signal *does* result from OCIO dissociation.

However, recent studies by Davis and Lee,¹¹ who measured the Cl yield from 350 to 475 nm by photofragment translational energy spectroscopy, found that the total yield of Cl production is only important near 404 nm, where a maximum of $3.9\% \pm 0.8\%$ is reached; the yield between 350 and 370 nm is below 0.2%. In order to explain these discrepancies, Davis and Lee suggested that the high yield in Bishenden's REMPI spectrum is due to photodissociation (by the probe laser) of the ClO product followed by REMPI (2+1) detection of Cl atoms within the time duration of the nanosecond-probe laser used in the experiments. A further result of their work is that the yield of

$\text{Cl} + \text{O}_2$ from symmetric stretch or symmetric stretch plus bend excitation is ~ 10 times greater than the yield from states at nearly the same energy with asymmetric stretch excitation. To explain this mode-specific behavior, it was proposed that the symmetric stretch and the bending modes favor coupling into the 2B_2 state whose equilibrium angle is near 90° (Fig. 2). On this state then, OCIO undergoes a concerted decomposition from a transition state geometry close to C_{2v} , rather than an isomerization process to form ClOO followed by a unimolecular dissociation. This is consistent with the theoretical analysis of Gole,¹ who suggested that vibronic coupling to nearby states plays an important role in the $\text{Cl} + \text{O}_2$ channel.

Glowia *et al.*⁵ have reported on the absorption, in a static gas cell, of OCIO in femtosecond pump-probe experiments. OCIO was excited by a pump pulse at 308 nm, while the ClO product was monitored by the absorption of a continuum probe pulse in the wavelength region between 268 and 278 nm. No ClO was detected on a time scale of up to 1 ns. Using a 308 nm nanosecond excimer laser as a pump and the femtosecond continuum laser as a probe, however, ClO absorption built up after several hundred nanoseconds. Vaida *et al.*, who detected the formation of ClO^+ within the nanosecond laser pulse at 308 nm, attributed the unexpected (very long) observed time scale of Glowia *et al.* to the collisional relaxation of the vibrationally excited ClO .⁷

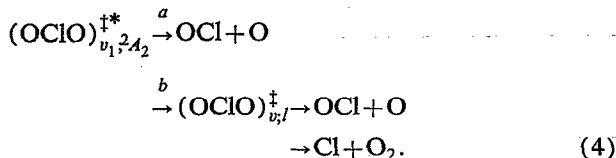
From the above discussion, the time scales for predissociation in the energy range up to $v_1 = 10$ are inferred from linewidth measurements. The yield of ozone-destroying Cl in this photodissociation process seems to be minor, especially in a wavelength regime below 370 nm. The corresponding predissociation mechanisms for this $\text{Cl} + \text{O}_2$ channel are interpreted in terms of various interactions of the initially excited A^2A_2 state with the two lower-lying 2A_1 and 2B_2 states. In what follows, we consider the femtosecond dynamics in the high-energy excitation regime of $v_1 = 11-17$. The observation of the femtosecond decay of the initially excited states gives direct measure of the dissociation. From the shape of the femtosecond transients and the energy dependence, we examine the mechanism and the dynamics of prompt OCIO dissociation to $\text{ClO} + \text{O}$ vs the indirect dissociation, involving nearby potentials, in the $\text{ClO} + \text{O}$ and $\text{Cl} + \text{O}_2$ channels.

B. Femtosecond dynamics and mechanism

The observed biexponential decay of OCIO over the entire range of v_1 studied indicates that the dynamics do not reflect a direct process only. There are a number of characteristics which assign the origin of the observed behavior. First, the decay constant of the fast component, which ranges from about 30 fs at $v_1 = 17$ to about 120 fs at $v_1 = 11$ is different from the two pulse cross correlation; as mentioned before, the cross correlation is symmetric, whereas the fast component is not. Second, the slow component of the decay, which ranges from about 300 fs at $v_1 = 17$ to about 500 fs at $v_1 = 11$, depends on the excitation energy. Third, the ratio of the fast to slow component, which does not change with intensity (pump or probe)

changes with ν_1 , but not when the pump is tuned within a specific ν_1 band (~ 4 nm range). From these observations, we conclude that the fast component is not an “off-resonance” transient peak, consistent with the fact that the pump is tuned to the strong absorption of the ν_1 bands and not to an off-resonance absorption region. The fact that we did not see a change in the transient behavior over a given range of ν_1 indicates that there is no mode selectivity at these high energies and that homogeneous dynamics from an initial state are operative. For example, one may attribute the fast component to a level involving the asymmetric stretch ClO+O products channel and the slow component to the symmetric stretch level which ultimately produces Cl+O₂. However, this assignment is inconsistent with the A/B ratio as the absorption of the ν_1 dominates, and also the yield for the Cl+O₂ channel at 350–370 nm is less than 0.2%.¹¹

The simplest mechanism to emerge involves the decay of the ν_1 state on the 2A_2 potential and the formation of intermediates of OCIO on the nearby PES(s). The reaction involves the following elementary steps:



The total rate of the initial decay is determined by both $a+b$ channels. Fundamentally, process a is the one described in Fig. 3. Excitation of the symmetric stretch is bound provided the system is along the line of the saddle (in a deterministic classical picture), but of course any motion (even zero-point motion) can take the system into the second dimension of the asymmetric stretch to yield OCl+O. In an adiabatic picture (and on one surface), ν_1 excitation in the transition-state region leads to ν'' excitation in OCl with a net translational energy for the recoil of OCl and O. We can estimate the time scale for this process based on the energetics, assuming a simple exponential repulsive potential. Taking the steepness of the potential to be 0.7 bohr (0.37 Å) (extrapolated from the asymmetric stretch coordinate in Fig. 2), and knowing that the translational energy release is about 1 eV (the excess energy above the OCl+O threshold minus the internal energy of OCl), the time for bond breakage [at 5.5 bohr (see Fig. 2)] is approximately 40 fs.^{20,21,39} Naturally, at least 2D calculations are needed for accurate comparisons.

The total rate for producing the intermediate(s) $(\text{OCIO})_{\nu_1, l}^{\dagger}$ in different vibrational levels (ν) of the lower-energy (l) PES(s) via channel b is determined by the effective coupling of the 2A_2 state to the nearby 2B_2 , 2A_1 , or to the ground state 2B_1 . Quantum mechanically, one must consider the coupling of the $|^2A_2, \nu_1\rangle$ level to the quasienergetic levels of the intermediate which then couple to the translational continuum of the OCl+O or Cl+O₂ channels. This type of coupling (see Fig. 11) can find analogies in the problems of intramolecular vibrational-energy redistribution (IVR) and nonradiative decay (for reviews, see Refs. 40 and 41). To compare with experimental rates, we

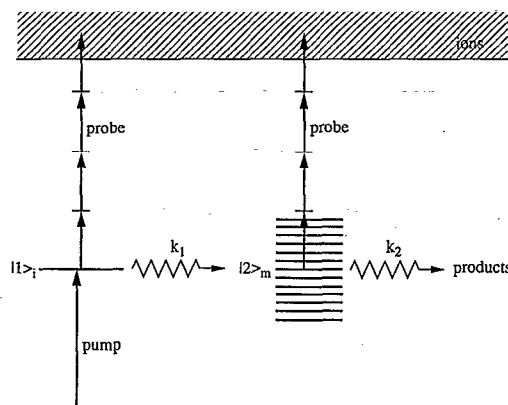


FIG. 11. The scheme for the coupling of the initial $(|1\rangle)_i$ state to a manifold $(|2\rangle)_m$ of levels, followed by a dissipative decay to translational continua (see the text).

adapt a simple kinetic model (biexponential decay) which captures the essence of the quantum treatment, keeping in mind that the fundamental limitation of the kinetic description is the absence of coherence.^{40,41} This type of two-step model has been invoked in describing similar biexponential behaviors associated with the dynamics of IVR in stilbene by MPI,²² IVR/predissociation of van der Waals complexes by fluorescence or MPI,^{24,42} and more recently for H-atom transfer.⁴³ Biexponential decay^{44,45} has also been observed in relation to interelectronic state coupling.⁴⁶

In the case of OCIO, the initial state $|^2A_2, \nu_1\rangle \equiv |1\rangle_i$ in Fig. 11) undergoes energy redistribution into the manifold of the lower-energy surfaces followed by the relatively slow overall decay of the “equilibrated” distribution to give products. Designating the decay constant of the initial non-stationary state by k_1 and the equilibrated distribution by k_2 , one can obtain an expression for the population change with time. Ionization out of the $(|1\rangle)_i$ state is described by an effective four-photon ionization cross section σ_1 , and by σ_2 for ionization out of the $(|2\rangle)_m$ manifold. Solving the corresponding rate equations leads to a molecular response function for the ion yield $M(t)$ as a function of pump-probe delay time (t) of the form

$$\begin{aligned}
 M(t) &= 0, \quad \text{for } t < 0, \\
 M(t) &= (\sigma_1 - \sigma_2 K) e^{-k_1 t} + \sigma_2 K e^{-k_2 t}, \quad \text{for } t \geq 0.
 \end{aligned} \quad (5)$$

In Eq. (5), the linear pump excitation is invoked and K is given by $k_1/(k_1 - k_2)$. The expression for $M(t)$ given here is related to $M(t)$ in Eq. (3) by $A = \sigma_1 - \sigma_2 K$, $B = \sigma_2 K$, $\tau_1 = 1/k_1$, $\tau_2 = 1/k_2$; the ratio A/B is given by $(\sigma_1/\sigma_2)[(k_1 - k_2)/k_1] - 1$. In Ref. 22, the explicit influence of a resonant intermediate for probing in this kind of model is investigated. It was found that only the ratio of the two rates is affected, not the rates themselves. For this reason, we describe our four-photon probe process by an effective ionization cross section, and the effect of the intermediate is discussed only when we consider power dependencies (*vide supra*). Note that we have neglected reversibility of $(|2\rangle)_m$ to $(|1\rangle)_i$ based on the relative density of states. However,

σ_1 should be on the order of $10\sigma_2$ for typical time constant and amplitude values (Fig. 9), otherwise the response function would not have an instantaneous rise. REMPI probing from two different electronic structures could explain different ionization cross sections⁴⁴ simply by different selection rules or ionization potentials for the four probe photons involved in the ionization process.⁴⁷

The nature of the $(\text{OCIO})_{v_1}^+$ intermediate depends on the potential. On the ground state 2B_1 , the intermediate is a vibrationally hot ground state molecule with energies of ~ 1 eV above dissociation (Fig. 2) to $\text{ClO} + \text{O}$. In C_{2v} , Herzberg–Teller vibronic coupling is allowed between 2A_2 and 2B_1 as the direct product contains the b_2 irreducible representation of the asymmetric stretch vibration. In Ref. 3, this route was considered less likely at lower energies because of the selectivity in line broadening with respect to the spin state prepared and the “large” density of states. At higher energies, the situation is different, particularly that the number of states is increased significantly. We can estimate the time scale for the decay of the “equilibrated” $(|2\rangle_m)$ distribution, described by k_2 , by calculating the rates based on microcanonical transition-state theories. This is similar to the treatment given in Ref. 48 for the dissociation of NCNO. However, since the energy above dissociation is large (~ 1 eV), we expect the transition state to be more of a tight type. Accordingly, we adopted the simple Rice–Ramsperger–Kassel–Marcus (RRKM) expression

$$k(E) = \frac{N^\ddagger(E - E_0)}{h\rho(E)} \quad (6)$$

for an order-of-magnitude estimate. In Eq. (6), $N^\ddagger(E - E_0)$ is the number of states in the transition state at energy E , excluding the reaction coordinate. E_0 denotes the reaction threshold, while $\rho(E)$ is the density of states of the reactant. The estimate was made by taking the vibrational frequencies from Peterson and Werner¹² (see also Table I) for the three electronic states under consideration (ignoring anharmonicities). E_0 was chosen to be D_0 for the X^2B_1 ground state. Taking the degeneracy of the problem into account (both bonds are equivalent), we multiplied the calculated rates by a factor of 2. Expressed in lifetimes, we obtain the following results by this estimate: the X^2B_1 state shows increasing decay times from 90 to 130 fs in the wavelength range from 310 to 350 nm. Similar estimates were made for the other states. Decay of the 2B_2 state results in a constant fragmentation time of about 30 fs in this energy range. The 2A_2 state shows an increase in the decay times from 30 to 50 fs.⁴⁹

The experimental observation of an increase of the slow time constant from about 300 fs at 310 nm excitation to about 500 fs at 350 nm excitation is in agreement with RRKM trends, which shows an increase of the decay time with decreasing excitation energy. The fact that tuning the pump laser in small energy ranges (up to 4 nm) did not affect the decay times is consistent with the interpretation that the biexponential decay is due to energy redistribution followed by a decay of a distribution of levels of the intermediate(s) formed. As mentioned above, the calculation of

$k(E)$ is intended to serve as an order-of-magnitude estimate and more accurate calculations, similar to those done on NCNO (Ref. 50), are underway. We also plan to compare with calculations made for analysis of the recent sub-picosecond study of NO_2 dissociation by the Wittig group.⁵¹ In the preliminary study of the OCIO–water clusters, we have observed the fast component, but the signal-to-noise ratio was not (yet) good enough to obtain an accurate ratio of A/B . It is consistent to see a fast (or faster) component as we expect the cluster modes to help the energy redistribution.

The $\text{Cl} + \text{O}_2$ products channel also involves the coupling of two potentials. The transition from the ground state 2B_1 to the 2A_2 state results in the promotion of an electron into an orbital (b_1) which is $\text{Cl}-\text{O}$ antibonding, but $\text{O}-\text{O}$ bonding. The bond angle decreases accordingly from 117° to $\sim 107^\circ$ and the $\text{Cl}-\text{O}$ bond length increases from 1.47 to 1.62 Å.¹ Even though the bond angle decreases, the increase in bond length requires very large amplitude motion for concerted $^1\text{O}_2 + \text{Cl}$ to occur. However, if the intermediate $(\text{OCIO})^+$ has some population on the 2B_2 surface, then this intermediate will be produced with a compressed angle of $\sim 90^\circ$ (see Fig. 2); the electronic coupling between 2A_2 and 2B_2 provides a sensible route for having the two oxygens closer to each other on the 2B_2 surface. (The 2A_1 state may be involved indirectly.) To break the bond, the molecule in the transition-state region of the 2B_2 surface, which is rather strained, will concertedly release a large amount of kinetic energy, consistent with the beam experiments of Davis and Lee.¹¹ However, the rate of crossing into this transition state will depend, at a given energy, on the vibrational energy redistribution on the 2B_2 surface and, in particular, on the bend time scale. If we relate (in part) our long decay (hundreds of femtoseconds depending on v_1) to such a crossing, then only a few bend motions (see Table I) are required, since the period is about 100 fs. Once the system gets into the transition-state region, within a vibrational period Cl and O_2 separate yielding the large release of kinetic energy. Because of this barrier crossing and downhill kinematic, the translational energy distribution will not reflect the rate. The initial state absorption linewidth measurement, even if homogeneous, as discussed below, will not give the dynamics of this or the 2B_1 intermediate.

The coupling of the 2A_2 to the 2B_2 potential is by spin-orbit coupling³ and is not allowed in C_{2v} by a Herzberg–Teller mechanism ($A_2 \otimes B_2 = b_1$). Also in C_s this coupling is not allowed. Thus, the interplay between the spin-orbit coupling to 2B_2 and the vibronic coupling to 2B_1 determines the nature of the intermediate, and at higher energies, where the 2B_1 density of states is increasing, vibronic coupling may become the dominant interaction. This brings to focus two points. First, the yield for $\text{Cl} + \text{O}_2$, as mentioned above, decreases considerably at higher energies. Second, asymmetric vibrational excitation decreases the yield of $\text{Cl} + \text{O}_2$ [promoted by the bending mode (see Ref. 11 and the previous section)] as this excitation represents a promoting mode to the $\text{ClO} + \text{O}$ channel via vibronic coupling. Additionally, the trapping of ClO in

matrices by Arkell *et al.*,⁵² which suggested¹ the isomerization of OCIO to ClOO, may be the result of an interesting change in dynamical time scale. With energy dissipation to phonons, the intermediate (e.g., 2B_2) could cool down and the rate of crossing the transition state would become slow enough to compete with isomerization into ClOO.

To be complete, we must address the linewidth problem. At the energies studied here, Vaida's group reported the high resolution spectrum (Fig. 10). From the fit of a rotational band contour, they inferred a width of ~ 4 ps for $v_1=10$ and indicated that these widths "saturate" giving a value of ~ 1 ps at 303 nm (v_1 between 18 and 19). Several points must be considered. The mechanism discussed above reflects "overlapping resonances" because of the coupling with lower-energy potentials. This results in a background and it is impossible to consider the system as homogeneously broadened in the sense of a two-level problem with $\Delta\bar{\nu}_{\text{width}} (\text{cm}^{-1}) = 1/(2\pi\tau)$ (for a Lorentzian line shape). Second, there is a finite convolution due to the inhomogeneous rotational distributions of both states. For $v_1=11$, as an example, the two components of OCIO decay are $\tau_1 \sim 120$ fs and $\tau_2 \sim 500$ fs. We therefore expect a broad component of 44 cm^{-1} and narrower resonances of 11 cm^{-1} within this envelope. The high-resolution linewidth has a large apparent width ($\sim 40 \text{ cm}^{-1}$) which is comparable to the 44 cm^{-1} broadening, but clearly does not give the separate true dynamics of the initial state and the intermediates (bond breakage).

An envelope of 44 cm^{-1} must be less than the $\Delta\bar{\nu}_1$ separation ($\sim 700 \text{ cm}^{-1}$) in order for the v_1 progression to be observed and "predissociation" to be identified. Indeed, this is experimentally true, and brings another important point—the excitation in the v_1 manifold is in the transition-state region of the 2A_2 potential. The v_1 "sharp" progression is therefore the (transverse) vibrational structure of the transition state,⁵³ and to be observed, the lifetime for motion along the asymmetric stretch must be longer than the symmetric stretch vibrational period. In the example given above, the spacing between the v_1 transitions is ~ 16 times greater than the width of an individual v_1 , indicating that the lifetime is longer than the symmetric vibrational period by a factor of ~ 3 (note that even if the lifetime and the vibrational period are the same, the ratio of the separation to linewidth is ~ 6 because of the 2π factor on going from lifetime to width). If the potential along the symmetric stretch is anharmonic, then the period will be even longer than that determined by the $v_1=1$ frequency. When there is separation of the symmetric stretch transitions, one speaks loosely of "predissociation," but it should be noted that this is not vibrational predissociation in its strict sense, where vibrational energy transfer is part of the dissociation dynamics [as, e.g., in the dissociation of van der Waals complexes (A_2-X)]. The analogy made here with excitations to the transition-state region is similar to the case of HgI_2 discussed above¹⁷⁻¹⁹ and to the photodetachment experiments of Neumark *et al.*⁵⁴ where direct absorption has been made. Butler has made this analogy between absorption and "resonance" dynamics recently.⁵⁵ For OCIO, the

initial transition-state region excitation and coupling with nearby surfaces are the two key dynamical features for the elementary fragmentation to $\text{ClO} + \text{O}$ and $\text{Cl} + \text{O}_2$.

V. SUMMARY AND CONCLUSIONS

This contribution presents femtosecond real-time studies of OCIO elementary fragmentation in a supersonic molecular beam. Mass-spectrometry detection has been used to identify the reactants, products, and some selective clusters of OCIO with water. These dissociation products ClO, O, and Cl (and the isomer ClOO) played an important role to the first millisecond flash photolysis experiments^{56,57} and to the ozone depletion problem.⁵⁸ Here, the wavelength range from 308 to 352 nm was covered, corresponding to symmetric stretch excitation of $v_1=17-11$. The parent ion OCIO^+ is observed here with femtosecond pulses, making it possible to monitor the initial dynamics of OCIO. This ion was not detected in nanosecond-laser REMPI experiments performed in this excitation energy range due to the efficient ultrafast photochemistry.

The observed decay shows a biexponential behavior; both time constants decrease with increasing excitation energy. The form of the transients and their change with energy reflects the reaction intermediates, and our analysis considers the nearby potentials (2B_2 , 2A_1) and the ground state (2B_1) as the source of interaction. In addition to the direct fragmentation to $\text{ClO} + \text{O}$, the dissociation proceeds through the intermediates to give the primary products $\text{ClO} + \text{O}$ on the ground state and/or the minor products $\text{Cl} + \text{O}_2$ on the 2B_2 state. The change in the relative yield, the kinetic energy release, and the increase or decrease in the rates with selective vibrational modes (e.g., bending or asymmetric vibrations) are consistent with our picture. Furthermore, the change in bonding upon excitation, the nature of the transition-state on both surfaces, and the calculated rates of the reaction support the conclusion. Some comments on the relevance of linewidth measurements are made, emphasizing the insensitivity of the width to the dynamics of the intermediates and the inhomogeneity due to overlapping resonances and rotational convolutions.

The observed ClO transient reflects two different contributions—ionic fragmentation, showing a similar (but time-shifted) transient as the parent OCIO at short delay times, and neutral fragmentation leading to a final nonzero value of ClO^+ at longer delay times. It was shown that the neutral fragmentation of OCIO excited by a femtosecond laser pulse at 308 nm leads to ClO formation on a time scale of a couple of hundred femtoseconds. Previous work reported no ClO appearance up to several hundred nanoseconds.

The preliminary studies of OCIO clusters with water $(\text{OCIO})_n(\text{H}_2\text{O})_m$ with n ranging from 1 to 3 and m from 0 to 3 opens up the possibility to study the heterogeneous photochemistry of these species in the time domain. We plan to extend the femtosecond dynamics studies reported here to these clusters and also to lower energies in isolated OCIO and the related systems of ClOCl and ClONO₂.⁵⁹

Theoretical wave packet 2D studies, similar to those made on IHGI,¹⁹ are part of these efforts.

ACKNOWLEDGMENTS

This work was supported by a grant from the National Science Foundation and from the Air Force Office of Scientific Research. We wish to thank Professor V. Vaida, Professor M. Okumura, and Professor J. Simon for stimulating discussions, and Dr. R. Friedl for his help in the sample preparation.

- ¹J. L. Gole, *J. Phys. Chem.* **84**, 1333 (1980).
- ²S. Michielsen, A. J. Merer, S. A. Rice, F. A. Novak, K. A. Freed, and Y. J. Hamada, *J. Chem. Phys.* **74**, 3089 (1981).
- ³D. A. McDonald and K. K. Innes, *Chem. Phys. Lett.* **59**, 562 (1987).
- ⁴E. C. Richard, T. W. Jones, and V. Vaida, *J. Phys. Chem.* **93**, 6346 (1989).
- ⁵J. H. Glowina, J. Misewich, and P. P. Sorokin, in *Supercontinuum Lasers*, edited by R. R. Alfano (Springer, Berlin, 1990), p. 370.
- ⁶W. G. Lawrence, K. C. Clemitshaw, and V. A. Apkarian, *J. Geophys. Res.* **95**, 18591 (1990).
- ⁷E. Ruehl, A. Jefferson, and V. Vaida, *J. Phys. Chem.* **94**, 2990 (1990).
- ⁸E. Bishenden, J. Haddock, and D. J. Donaldson, *J. Phys. Chem.* **95**, 2113 (1991).
- ⁹E. C. Richard and V. Vaida, *J. Chem. Phys.* **94**, 153 (1991).
- ¹⁰E. C. Richard and V. Vaida, *J. Chem. Phys.* **94**, 163 (1991).
- ¹¹H. F. Davis and Y. T. Lee, *J. Phys. Chem.* **96**, 5681 (1992).
- ¹²K. A. Peterson and H. J. Werner, *J. Chem. Phys.* **96**, 8948 (1992).
- ¹³V. Vaida, E. C. Richard, A. Jefferson, L. A. Cooper, R. Flesch, and E. Ruehl, *Ber. Bunsenges. Phys. Chem.* **96**, 391 (1992).
- ¹⁴V. Vaida, S. Solomon, E. C. Richard, E. Ruehl, and A. Jefferson, *Nature* **342**, 405 (1989).
- ¹⁵A. Wahner, G. S. Tyndall, and A. R. Ravishankara, *J. Phys. Chem.* **91**, 2734 (1987).
- ¹⁶D. S. Bethune, A. J. Schell-Sorokin, J. R. Lankard, M. M. T. Loy, and P. P. Sorokin, in *Advances in Laser Spectroscopy*, edited by B. A. Garetz and J. R. Lombardi (Heyden, Philadelphia, 1983), Vol. 2, p. 1.
- ¹⁷R. M. Bowman, M. Dantus, and A. H. Zewail, *Chem. Phys. Lett.* **156**, 131 (1989).
- ¹⁸M. Dantus, R. M. Bowman, M. Gruebele, and A. H. Zewail, *J. Chem. Phys.* **91**, 7437 (1989).
- ¹⁹M. Gruebele, G. Roberts, and A. H. Zewail, *Philos. Trans. R. Soc. London Ser. A* **332**, 35 (1990).
- ²⁰L. R. Khundkar and A. H. Zewail, *Annu. Rev. Phys. Chem.* **41**, 15 (1990).
- ²¹A. H. Zewail, *Faraday Discuss. Chem. Soc.* **91**, 207 (1991).
- ²²J. W. Perry, N. F. Scherer, and A. H. Zewail, *Chem. Phys. Lett.* **103**, 1 (1983).
- ²³L. R. Khundkar and A. H. Zewail, *Chem. Phys. Lett.* **142**, 426 (1987).
- ²⁴J. L. Knee, L. R. Khundkar, and A. H. Zewail, *J. Chem. Phys.* **87**, 116 (1987).
- ²⁵T. Baumert, M. Grosser, R. Thalweiser, and G. Gerber, *Phys. Rev. Lett.* **67**, 3753 (1991).
- ²⁶M. Dantus, M. H. M. Jansen, and A. H. Zewail, *Chem. Phys. Lett.* **181**, 281 (1991).
- ²⁷M. J. Rosker, M. Dantus, and A. H. Zewail, *J. Chem. Phys.* **89**, 6113 (1988).
- ²⁸R. I. Derby and W. S. Hutchinson, *Inorg. Synth.* **4**, 152 (1953).
- ²⁹R. Flesch, E. Ruehl, K. Hottmann, and H. Baumgaertel, *J. Phys. Chem.* **97**, 837 (1993).
- ³⁰N. Basco and R. D. Morse, *Proc. R. Soc. London Ser. A* **336**, 495 (1974).
- ³¹L. P. Fischer, *Trans. Faraday Soc.* **63**, 684 (1967).
- ³²J. A. Coxon, *Can. J. Phys.* **57**, 1538 (1979).
- ³³T. Baumert, V. Engel, C. Meier, and G. Gerber, *Chem. Phys. Lett.* **200**, 488 (1992).
- ³⁴D. K. Bulglin, J. M. Dyke, N. Jonathan, and A. J. Morris, *J. Chem. Soc. Faraday Trans. 2* **75**, 456 (1978).
- ³⁵G. Herzberg, *Molecular Spectra and Molecular Structure. III. Electronic Spectra and Electronic Structure of Polyatomic Molecules* (Van Nostrand, New York, 1966).
- ³⁶E. W. Schlag and H. J. Neusser, *Acc. Chem. Res.* **16**, 355 (1983).
- ³⁷D. P. Taylor and P. M. Johnson, *J. Chem. Phys.* **98**, 1810 (1993) and references therein.
- ³⁸T. Baumert, R. Thalweiser, V. Weiss, and G. Gerber, *Z. Phys. D* **26**, 131 (1993).
- ³⁹Q. Liu and A. H. Zewail, *J. Phys. Chem.* **97**, 2209 (1993).
- ⁴⁰P. Felker and A. H. Zewail, *Adv. Chem. Phys.* **87**, 265 (1988) and references therein.
- ⁴¹J. Kommandeur, W. A. Majewski, W. L. Meerts, and D. W. Pratt, *Annu. Rev. Phys. Chem.* **38**, 433 (1987) and references therein.
- ⁴²D. H. Semmes, J. S. Baskin, and A. H. Zewail, *J. Chem. Phys.* **92**, 3359 (1990).
- ⁴³J. L. Herek, S. Pedersen, L. Bañares, and A. H. Zewail, *J. Chem. Phys.* **97**, 9046 (1992).
- ⁴⁴J. L. Knee, F. E. Doany, and A. H. Zewail, *J. Chem. Phys.* **82**, 3359 (1985).
- ⁴⁵A. Lorincz, D. D. Smith, F. Novak, R. Kosloff, D. J. Tannor, and S. A. Rice, *J. Chem. Phys.* **82**, 1067 (1985).
- ⁴⁶J. L. Knee, L. R. Khundkar, and A. H. Zewail, *J. Phys. Chem.* **89**, 3201 (1985).
- ⁴⁷For pure IVR on one PES, biexponential decay is also predicted (Ref. 40). However, one does not obtain selectivity in ionization from the initial and final vibrational levels unless intermediate states are involved, or near-threshold ionization is used as selective means for the FC factors. In the case of OCIO, there was no change in form of transients over the energy range studied; this fact is hard to reconcile with IVR on one surface. It should be noted that for the coupling scheme of two surfaces (Fig. 11), if we consider reversibility, then a biexponential decay is also predicted even if the initial state is the only one ionized. Because of the relative density of states, we invoked MPI out of the two states, but this is not cardinal if reversibility is strong.
- ⁴⁸L. R. Khundkar, J. L. Knee, and A. H. Zewail, *J. Chem. Phys.* **87**, 77 (1987).
- ⁴⁹The calculations were performed using the Whitten-Rabinovich approximation and compared to a direct count RRRM routine provided by C. Lienau from Prof. J. Troe group. Both programs gave the same result. For example, at 310 nm, $\rho(E) = 1.18/\text{cm}^{-1}$ and $N^{\ddagger} = 212$, where at 350 nm, $\rho(E) = 0.9/\text{cm}^{-1}$ and $N^{\ddagger} = 114$ for the X^2B_1 state. In the direct count, we obtained $\rho(E)$ according to $\rho(E) = [1/(\Delta\nu)] \sum_{i=1}^{\infty} \rho_i(E_i)$, where $\Delta\nu$ is the laser bandwidth (cm^{-1}) and $\rho_i(E_i)$ is the density of states per cm^{-1} , in increments of 1 cm^{-1} .
- ⁵⁰S. J. Klippenstein, L. R. Khundkar, A. H. Zewail, and R. A. Marcus, *J. Chem. Phys.* **89**, 4761 (1988).
- ⁵¹G. A. Brucker, S. I. Ionov, Y. Chen, and C. Wittig, *Chem. Phys. Lett.* **194**, 301 (1992).
- ⁵²A. Arkell and I. Schwager, *J. Am. Chem. Soc.* **89**, 5999 (1967).
- ⁵³S. Pedersen, L. Bañares, and A. H. Zewail, *J. Chem. Phys.* **97**, 8801 (1992).
- ⁵⁴D. M. Neumark, *Annu. Rev. Phys. Chem.* **42**, 153 (1992) and references therein.
- ⁵⁵L. J. Butler, *Chem. Phys. Lett.* **182**, 393 (1991).
- ⁵⁶G. Porter and F. J. Wright, *Discuss. Faraday Soc.* **14**, 23 (1953).
- ⁵⁷G. Porter, in *The Chemical Bond—Structure and Dynamics*, edited by A. H. Zewail (Academic, San Diego, 1992), p. 113.
- ⁵⁸H. S. Johnston, *Annu. Rev. Phys. Chem.* **43**, 1 (1992) and references therein.
- ⁵⁹T. K. Minton, C. M. Nelson, T. A. Moore, and M. Okumura, *Science* **258**, 1342 (1992).
- ⁶⁰A. W. Richardson, R. W. Redding, and J. C. D. Brand, *J. Mol. Spectrosc.* **29**, 93 (1969); see also Ref. 61.
- ⁶¹R. F. Curl, Jr., R. F. Heidelberg, and J. L. Kinsey, *Phys. Rev.* **125**, 1993 (1962).
- ⁶²The rotational constants of OCIO have been determined in Ref. 60 and references therein. Relevant to this work, from the available data, we calculate the rotational dephasing (Ref. 63) based on the values of the constants $A = 1.056 \text{ cm}^{-1}$, $B = 0.309 \text{ cm}^{-1}$ and $C = 0.281 \text{ cm}^{-1}$. At a rotational temperature of $\sim 50 \text{ K}$, we calculate a dephasing time of $\sim 1 \text{ ps}$, longer than the observed time scales of the decay. This indicates the insignificance of the rotational contribution to the initial decay. The lack of large polarization anisotropy on the signal is most likely due to the four-photon MPI mode of probing.
- ⁶³P. M. Felker and A. H. Zewail, *J. Chem. Phys.* **86**, 2460 (1987).